Hindawi
Journal of Nanomaterials
Volume 2017, Article ID 3659423, 11 pages
https://doi.org/10.1155/2017/3659423

Research Article

Rapid Detection and Identification of miRNAs by Surface-Enhanced Raman Spectroscopy Using Hollow Au Nanoflowers Substrates

Xiaowei Cao,[1,2,3,4] Min Bao,[1,2] Yibo Shan,[1,2] Wei Li,[1,2] and Hongcan Shi[1,2,5]

[1] *Institute of Translational Medicine, Medical College, Yangzhou University, Yangzhou 225001, China*
[2] *Department of Integrative Traditional & Western Medicine, Medical College, Yangzhou University, Yangzhou 225001, China*
[3] *Jiangsu Coinnovation Center for Prevention and Control of Important Animal Infectious Diseases and Zoonoses, Yangzhou University, Yangzhou 225009, China*
[4] *Jiangsu Key Laboratory of Zoonosis, Yangzhou University, Yangzhou 225009, China*
[5] *Jiangsu Key Laboratory of Experimental & Translational Noncoding RNA Research, Medical College, Yangzhou University, Yangzhou 225001, China*

Correspondence should be addressed to Hongcan Shi; shihongcan@yzu.edu.cn

Received 18 June 2017; Accepted 30 August 2017; Published 19 October 2017

Academic Editor: Krishna Kant

MicroRNAs (miRNAs) are recognized as regulators of gene expression during the biological processes of cells as well as biomarkers of many diseases. Development of rapid and sensitive miRNA profiling methods is crucial for evaluating the pattern of miRNA expression related to normal and diseased states. This work presents a novel hollow Au nanoflowers (HAuNFs) substrate for rapid detection and identification of miRNAs by surface-enhanced Raman scattering (SERS) spectroscopy. We synthesized the HAuNFs by a seed-mediated growth approach. Then, HAuNFs substrates were fabricated by depositing HAuNFs onto the surfaces of (3-aminopropyl)triethoxysilane- (APTES-) functionalized ITO glass. The result demonstrated that HAuNFs substrates had very good reproducibility, homogeneous SERS activity, and high SERS effect. The substrates enabled us to successfully obtain the SERS spectra of miR-10a-5p, miR-125a-5p, and miR-196a-5p. The difference spectra among the three kinds of miRNAs were studied to better interpret the spectral differences and identify miRNA expression patterns with high accuracy. The principal component analysis (PCA) of the SERS spectra was used to distinguish among the three kinds of miRNAs. Considering its time efficiency, being label-free, and its sensitivity, the SERS based on HAuNFs substrates is very promising for miRNA research and plays an important role in early disease detection and prevention.

1. Introduction

MicroRNAs (miRNAs) are small (19–25 nucleotides), non-coding, regulatory RNAs that play critical regulatory roles in almost every biological processes [1, 2]. Some studies concluded that approximately one-third to one-half of human genes are directly regulated by miRNAs with each miRNA predicted to target several hundred transcripts, making miRNAs one of the largest families of gene regulators [3]. miRNAs are implicated in the regulation of various cellular processes, including proliferation, metastasis, differentiation, and apoptosis [4]. The accumulating evidence has shown that miRNAs or patterns of miRNAs expressed may serve as biomarkers for a number of diseases and genetic disorders, particularly in the development of cancers [5, 6]. For example, Huo et al. found that miR-10a-5p have good predictive value in assessing the 28-day mortality of patients with sepsis [7]. Zhi et al. reported that miR-10a-5p may serve as a biomarker useful to improving the management of acute myeloid leukemia patients [8]. The similar results were reported in the cervical cancer [9, 10]. Zhong et al. found that miR-125a-5p inhibited the proliferation and invasion of lung cancer cells and facilitated lung cancer cell apoptosis [11]. Moreover miR-125a-5p expression was found to be associated with the age of breast cancer patients [12]. Li et al. reported

that overexpression of miR-196a-5p is associated with lymph node metastasis and clinical stage in gastric cancer [13]. The expression pattern of cancer-specific miRNAs has been identified in almost every type of cancer. Thus, miRNA expression profiles may be used for cancer diagnostics and classification, whereas current methods which are capable of detecting and profiling miRNA expression have limitations in sensitivity and breadth due to the short size, low abundance, and sequence similarity between miRNA family members [14]. The development of fast, sensitive, and efficient methods for identification of miRNAs has been of great importance for discovery of potential biomarkers of disease pathogenesis and for high-throughput detection of miRNAs expression profiles related to disease status.

Surface-enhanced Raman scattering (SERS) spectroscopy is a powerful spectroscopic detection technique that can enormously enhance the Raman signals of molecules adsorbed on or near the roughened surfaces of metallic nanostructured substrates. The detection sensitivity of SERS is 6–14 orders of magnitude higher than conventional Raman spectroscopy and is similar to fluorescence technique [15]. SERS can obtain rich molecular and structural information to identify biological samples with the vibrational fingerprints [16]. SERS also has many significant advantages over other technologies, such as its narrow spectral band, nondestruction, and weak Raman signal of water [17]. Therefore, it is very suitable for study of biomolecule in vitro. Ag and Au metallic materials are commonly used as SERS-active substrates [18]. Theoretically, their SERS enhancement effects mainly result from the "hot spots," which originate from the rough surface of nanoparticles and the gaps between metallic nanoparticles [19, 20].

Among all metallic nanoparticles, hollow Au nanoflowers (HAuNFs), with internal hollow cavity and external multiple sharp branches, have received a great deal of attention in the fields of materials science. The localized surface plasmon resonance (LSPR) of HAuNFs may be tuned between the visible and the near infrared (NIR) wavelengths by changing the size, branches, and shell thickness [21]. It showed that the LSPR of HAuNFs was of higher sensitivity than that of other nanoparticles. HAuNFs have high surface to volume ratios and their many branches which served as potential "hot spots" greatly enhance the electromagnetic field around the particle, both of which are beneficial for highly efficient SERS application [22]. In order to obtain greater sensitivity and signal enhancement, a variety of nanoparticles have been assembled into solid substrates (such as graphite, silicon, and ITO glass) by template method, self-assembly, nanosphere lithography, and electrochemical deposition. Recently, SERS has been used for biosensing virus, bacteria, proteins, and nucleic acid [23, 24]. Khlebtsov et al. fabricated centimeter-scale gold nanoisland films as reproducible SERS substrates for highly sensitive detection of the thiram fungicide in apple peels [25]. Sun et al. developed a promising magnetic SERS immunosensor to analyze intact but inactivated influenza virus H_3N_2 by constructing a sandwich complex consisting of SERS tags, target influenza viruses, and highly SERS-active magnetic supporting substrates [26]. Ouyang et al. proposed a laser wrapped graphene-Ag array for detection of methylated DNA and its oxidation derivatives by SERS [27]. However, widespread applications of SERS remain limited because of a lack of spectral reproducibility linked to the SERS substrate used to detect the sample. Furthermore, the surfactants and reductants on the surface are difficult to remove, which will severely interfere with the SERS results.

Table 1: Sequences of three kinds of miRNAs.

miRNAs	Sequence
miR-10a-5p	UACCCUGUAGAUCCGAACUGUG
miR-125a-5p	UCCCUGAGACCCUUUAACCUGUGA
miR-196a-5p	UAGUAGUUUCACUGUGAUUCGGG

In this study, employing the HAuNFs-decorated indium tin oxide (ITO) glass as a enhancing substrate, we applied SERS spectroscopy to classify miRNAs (Scheme 1). HAuNFs were assembled onto the surface of (3-aminopropyl)triethoxysilane- (APTES-) functionalized ITO glass slip by the sedimentary self-assembly method. We evaluated the SERS stability, homogeneity, and SERS effect of HAuNFs substrates. Then, SERS spectra of three kinds of miRNAs (miR-125a-5p, miR-196a-5p, and miR-10a-5p) were directly detected in near-real time, which could recognize the distinctive vibrational features of the structural characteristics of miRNA. The differences among these highly similar miRNAs have been well compared and distinguished through difference spectra analysis and principal component analysis (PCA) analysis. HAuNFs SERS substrates featuring rapid, label-free, and high sensitivity could serve as a promising tool for the ribonucleic acid analysis.

2. Materials and Methods

2.1. Materials. Chloroauric acid tetrahydrate ($HAuCl_4 \cdot 4H_2O$), silver nitrate ($AgNO_3$), trisodium citrate ($C_6H_5Na_3O_7 \cdot 2H_2O$), and hydroquinone (98%) were all purchased from Yangzhou Younuo Chemicals Co., Ltd. (China). The (3-aminopropyl)triethoxysilane and Nile blue A (NBA) were purchased from Yangzhou Noah Chemical Co., Ltd. (China). All glassware used was cleaned with aqua regia and deionized water. miRNA sequence was based on miRBase (microrna.sanger.ac.uk). Following the principle, the use of ABI's Primer Express software for primer design was synthesized by the Shanghai bioengineering technology company (Table 1).

2.2. Synthesis of HAuNFs. HAuNFs were synthesized by a seed-mediated growth approach, using hydroquinone and sodium citrate as reduction agents. During the synthesis of HAuNFs, galvanic reaction firstly happened between $HAuCl_4$ and Ag seeds in the reaction solution. As a result, Ag seeds gradually depleted off, which was due to the rate of Ag^+ diffusion being more than the rate of the Au contraction, thus forming hollow nanoshells structure. Secondly, Au^{3+} was reduced to Au^0 on the surface of nanoshells when adding reduction agents in reaction system. Au could continue

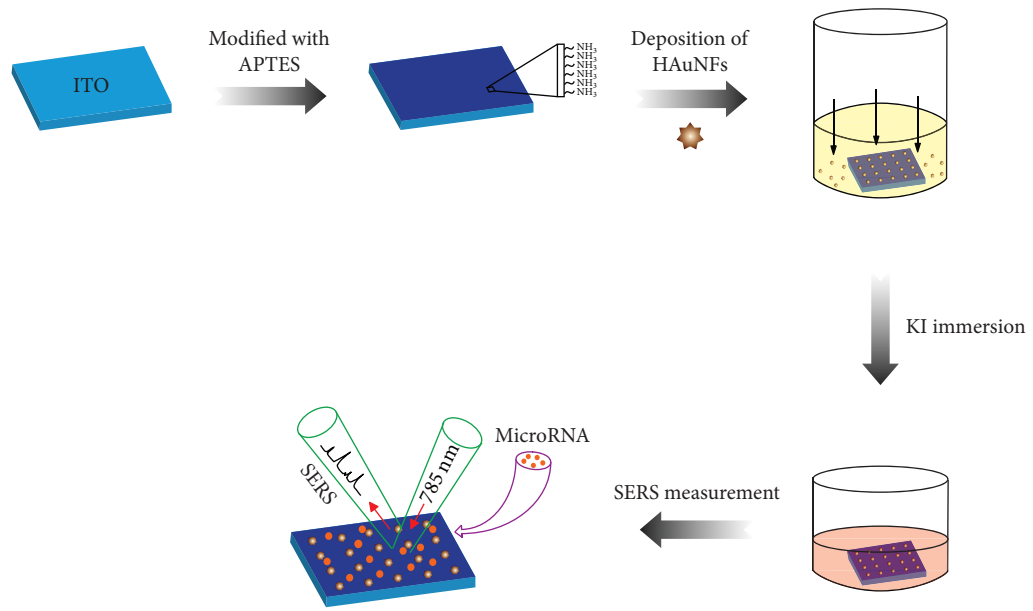

Scheme 1: Schematic illustration of fabricated process of HAuNFs substrate and SERS is used for detection and identification of miRNAs.

to pile up and grow on the rough surface because of the excess chloroauric acid. Finally, the flower-like, hollow Au nanoparticles were synthesized.

Ag seeds were prepared as previously reported. Briefly, 100 mL of 1 mM $AgNO_3$ solution was heated to boiling while being vigorously stirred. 1.5 mL of 1% citrate solution was injected into the boiling reaction mixture. The reaction was allowed to proceed for 1 h, after which the mixture was cooled to room temperature. Next, 0.5 mL of citrate-stabilized Ag seed solution was put into 10 mL deionized water in a glass vial under continuous stirring. Then, 200 μL 1% $HAuCl_4$ was mixed with above solution for 20 min to form Au nanoshells. Finally, 50 μL of 1% sodium citrate and 1 mL of 30 mM hydroquinone were sequentially added one by one, and, after 30 min, its color turned from yellow to black-green. The product was centrifuged twice at 5000 rpm for 10 min and was washed with deionized water.

2.3. Assembly of HAuNFs on APTES-Functionalized ITO. The fabrication process of HAuNFs substrate was described in Scheme 1. An ITO glass slip was washed with acetone and ultrapure water in the given order. The slip was further cleaned in ethanol for three times and dried at 70°C for 2 h in an air oven. The cleaned ITO glass slip was then immersed in 1% (v/v) ethanol solution of APTES in anhydrous ethanol for 24 h to form a self-assembled layer followed by thorough rinsing with ethanol and air-drying. Subsequently, the APTES-functionalized ITO glass slip was placed horizontally in the HAuNFs colloidal solution for 24 h. HAuNFs could be deposited onto the surfaces of APTES-functionalized ITO to obtain HAuNFs layer. The thiol moiety of APTES covalently binds to the substrate while its pendant primary amine group covalently binds to the nanoparticles. Finally, HAuNFs substrate was dipped into a solution containing 0.1 M KI solution for 10 min. The substrates were washed with ethanol and ultrapure water and were dried for 30 min at 30°C. Thus, the clean HAuNFs SERS substrates were obtained.

2.4. Instruments. The ultraviolet-visible-near infrared (UV-vis-NIR) spectrum was measured by a Cary UV-5000 spectrometer (Agilent). Transmission electron microscope (TEM) images were performed by a Tecnai 12 transmission electron microscope operating at an accelerating voltage of 60 kV (Philips). The surface morphology was recorded on a S-4800 II field-emission scanning electron microscope (FE-SEM) operated at 3.0 kV (Hitachi). Energy dispersive spectra (EDS) were obtained from a Siemens D5005. The dark-field images were collected using an inverted Olympus IX70 microscope with a highly numerical dark-field condenser.

2.5. SERS Measurements. SERS measurements were performed by a Raman spectrometer with a 50x working distance objective lens (Renishaw). The Raman shift was calibrated using the signal of 520 cm^{-1} from a silicon wafer. The laser powers focused on samples (NBA, miR-10a-5p, miR-125a-5p, and miR-196a-5p) were 5 mW for 785 nm and integration time of 10 s. Before SERS spectra collection, NBA solution was diluted to various concentrations ranging from 1×10^{-6} M to 1×10^{-12} M. For SERS measurement of miRNA, each miRNA was dropped directly on the prepared HAuNFs substrate and then subjected to Raman spectroscopy. The measured SERS spectra of 10 different points were used to obtain average SERS spectrum of miRNA.

2.6. Examining the EF. The enhancement factor (EF) of HAuNFs was calculated by the approach developed by Le Ru et al. [28], $EF = (I_{SERS}/C_{SERS})/(I_{RS}/C_{RS})$, where I_{SERS} corresponds to the SERS intensity obtained for the HAuNFs colloidal dispersion under a certain concentration C_{SERS} of

analyte and I_{RS} corresponds to the Raman intensity obtained under non-SERS conditions at analyte concentration of C_{RS}. NBA was used as analyte and the characteristic peak appeared at 592 cm^{-1} [29]. During the experimental process, the HAuNFs colloidal dispersion was mixed with the same volume of NBA for 4 h at 4°C, giving a final concentration with 10^{-6} M. When using $C_{SERS} = 10^{-6}$ M and $C_{RS} = 1 \times 10^{-2}$ M and the intensities measured, we can obtain the EF of HAuNFs.

3. Results and Discussion

3.1. HAuNFs Characterization. Figures 1(a) and 1(b) showed the UV-vis-NIR spectra of the Ag seeds and HAuNFs. At initial stages, Ag seeds displayed a strong absorption peak at 420 nm (Figure 1(a)). In the presence of the reductants, the Ag seeds continued to grow into HAuNFs, which had a strong absorption peak at about 750 nm (Figure 1(b)). The plasmon of HAuNFs in the NIR region shows their great potential for in vivo application. Figure 1(d) showed typical SEM and TEM images of the as-synthesized HAuNFs. The HAuNFs were well dispersed as individual entities, which could be prepared by large scale. The average diameter of HAuNFs was about 150 nm, and their rough surface contained many short, irregular, and obtuse branches. TEM image (see inset image in Figure 1(d)) exhibited that HAuNFs were hollow essence. It indicated that Ag seed at the center of the nanoparticle have been removed. As shown in Figure 1(e), the EDS result of the HAuNFs indicated the existence of silver, gold, carbon, and silicon and oxygen elements. The signals of silicon were attributed to the silicon wafer with a thin layer of silicon dioxide. The products were basically HAuNFs and small number of products was Au-Ag alloy. Raman spectra of NBA (Figure 1(f), black curve) and NBA-labeled AuNSs (Figure 1(f), red curve) were recorded under our experimental condition (785 nm laser line, 10 s integration time). NBA-labeled HAuNFs generated a strong Raman signals. Then, the SERS EF of HAuNFs was calculated by using the following expression, $EF = (I_{SERS}/C_{SERS})/(I_{RS}/C_{RS})$. SERS EF of HAuNFs is 4.3×10^5, which is much higher than EF (1×10^5) of Au nanostars reported by Nalbant Esenturk and Hight Walker [30].

3.2. Fabrication of HAuNFs Substrates. HAuNFs substrates were fabricated by the sedimentary self-assembly method, which do not need complicated equipment and are preponderant in commercial manufacture. During the experiment, APTES was used to make the pendant -NH_2 group of ITO glass slip, which could immobilize HAuNFs onto the substrate via Au-N covalent bonding [31]. Figure 2(a) revealed the SEM image of HAuNFs substrates. HAuNFs had slight aggregation and uniformly distributed on the ITO glass surface. The inset in Figure 2(a) was digital photograph of HAuNFs substrates, which had dark black-green with uniform colors. Dark-field microscopy is a widely used technique for imaging plasmonic particles, which cannot be observed in bright field. Figure 2(b) showed the dark-field image of HAuNFs substrates. HAuNFs strongly scatter yellow light due to their strong localized surface plasmon oscillation with a frequency in the NIR region [32]. In order to investigate the uniformity of the surface SERS signal, a SERS mapping experiment was performed by the Renishaw Raman microspectroscopy system. Figure 2(c) showed the SERS mapping of HAuNFs substrates, using the characteristic peak of NBA at 592 cm^{-1} as the mapping signal. The scan area was 40×50 mm^2, the step size was 2 mm, the laser power was 5 mW, and the acquisition time at each point was 10 s. The color of SERS mapping was used to display the intensity of the 592 cm^{-1} at each point according to a color scheme ranging from blue (lowest intensity) through red, orange, yellow, and red (highest intensity). From Figure 2(d), the deviation of SERS intensities at the strongest point (Figure 2(c)-A) to the weakest point (Figure 2(c)-B) was less than 10%, which supported the good homogeneity of the HAuNFs substrates.

UV-vis-NIR spectrum of HAuNFs substrates was shown in Figure 1(c). Compared with the UV-vis-NIR spectrum of colloidal HAuNFs solution, the absorption peak of HAuNFs substrates had a ~18 nm red shift, which might be caused by the changes of the distance between the particles and slight aggregation when assembled onto ITO glass surface. We further investigated the reproducibility of SERS signal of the NBA-labeled HAuNFs substrates. Three substrates, made at different time, were measured and shown in Figure 3(a). The deviation of peak intensity at 592 cm^{-1} is 5.2%, showing the substrates were made with good reproducibility. In addition to the uniformity and reproducibility of the substrates, the SERS stability of HAuNFs substrates was also tested (Figure 3(b)). HAuNFs substrates were stored for an extended period of time at room temperature. No significant changes in the SERS spectral peak and shape were observed, indicating the HAuNFs substrates had a very stable SERS enhancement effect. After 20 days, the SERS intensity at 592 cm^{-1} was only reduced by 8.7% compared with that of 0 days (see inset image in Figure 3(b)). Figure 3(c) showed the SERS spectra of various concentrations of NBA on HAuNFs substrates. The lower concentration of NBA solutions on HAuNFs substrates showed a silence of SERS signal, and thus the concentration of 1×10^{-12} M was known as the limit of detection for the NBA molecules. Furthermore, a little of surfactants and reductants remained on the surface of as-prepared HAuNFs substrates, characterized by some Raman bands and shown in Figure 3(d) (red curve). To reduce their interference with SERS detection of miRNA, the substrates were rinsed with a fresh 0.1 M KI solution. Iodide can be strongly adsorbed on Au surfaces though Au-I bond and easily replace the existing impurities, showing a clean background in SERS spectra in Figure 3(d) (black curve) [33]. Thus, iodide protected substrates can be conveniently used for direct detection of miRNAs.

3.3. SERS Spectral Analysis. To evaluate the sensitivity of HAuNFs substrates for miRNA detection, we have studied the SERS spectra of diluted miR-125a-5p samples with different concentrations adsorbed on the HAuNFs substrates (Figure 4(a)). Meanwhile, the SERS intensity at 733 cm^{-1} for diluted miR-125a-5p with different concentrations was

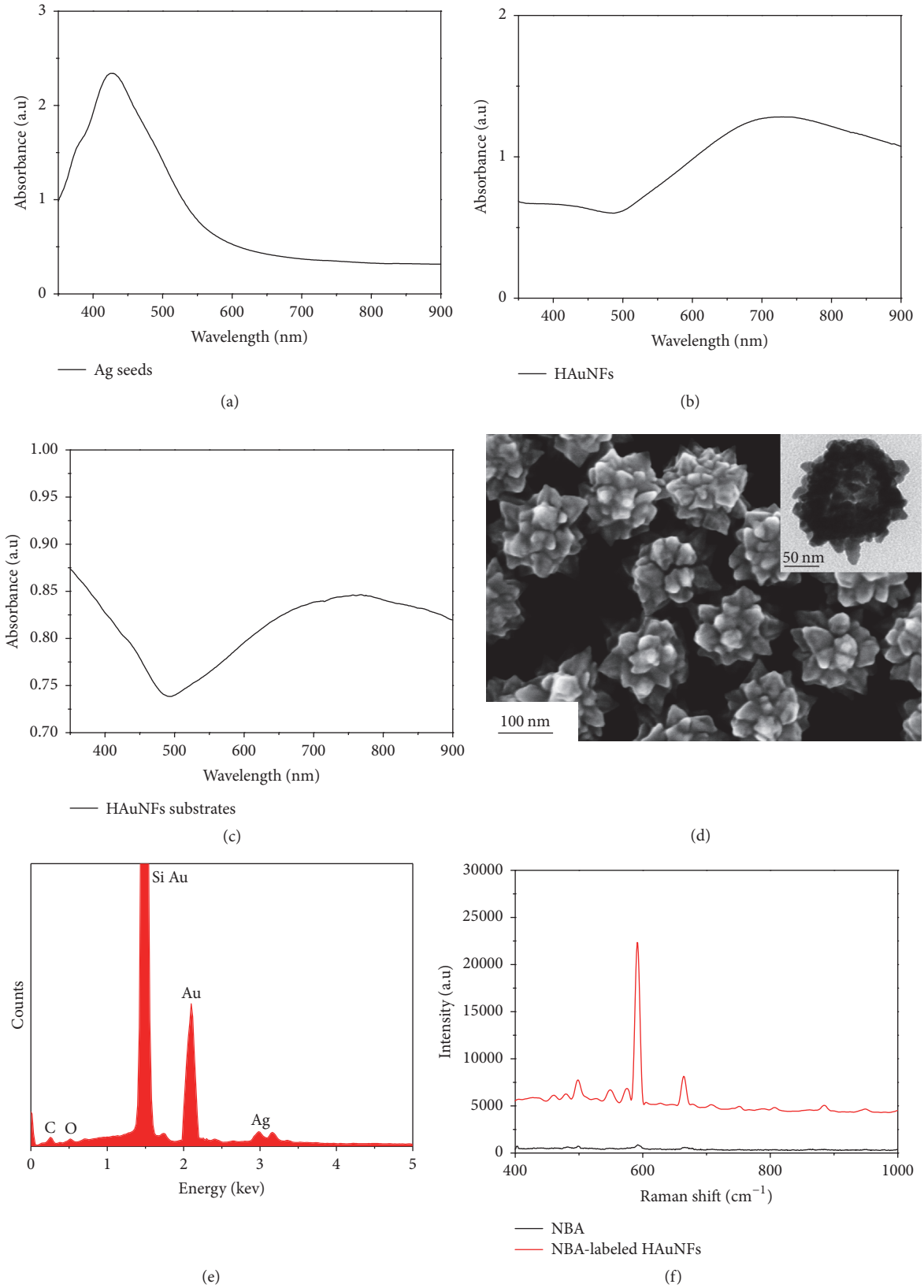

Figure 1: UV-vis-NIR spectra of (a) Ag seeds, (b) HAuNFs, and (c) HAuNFs substrate. (d) SEM image of HAuNFs. Inset TEM image shows the internal structure of HAuNFs. Scale bars: 100 nm and 50 nm for the SEM image and TEM image, respectively. (e) EDS spectrum of HAuNFs. (f) SERS spectrum of (black curve) NBA and (red curve) HAuNFs colloidal dispersion mixed with NBA under 785 nm excitation. The integration time was 10 s and laser intensity was 5 mW.

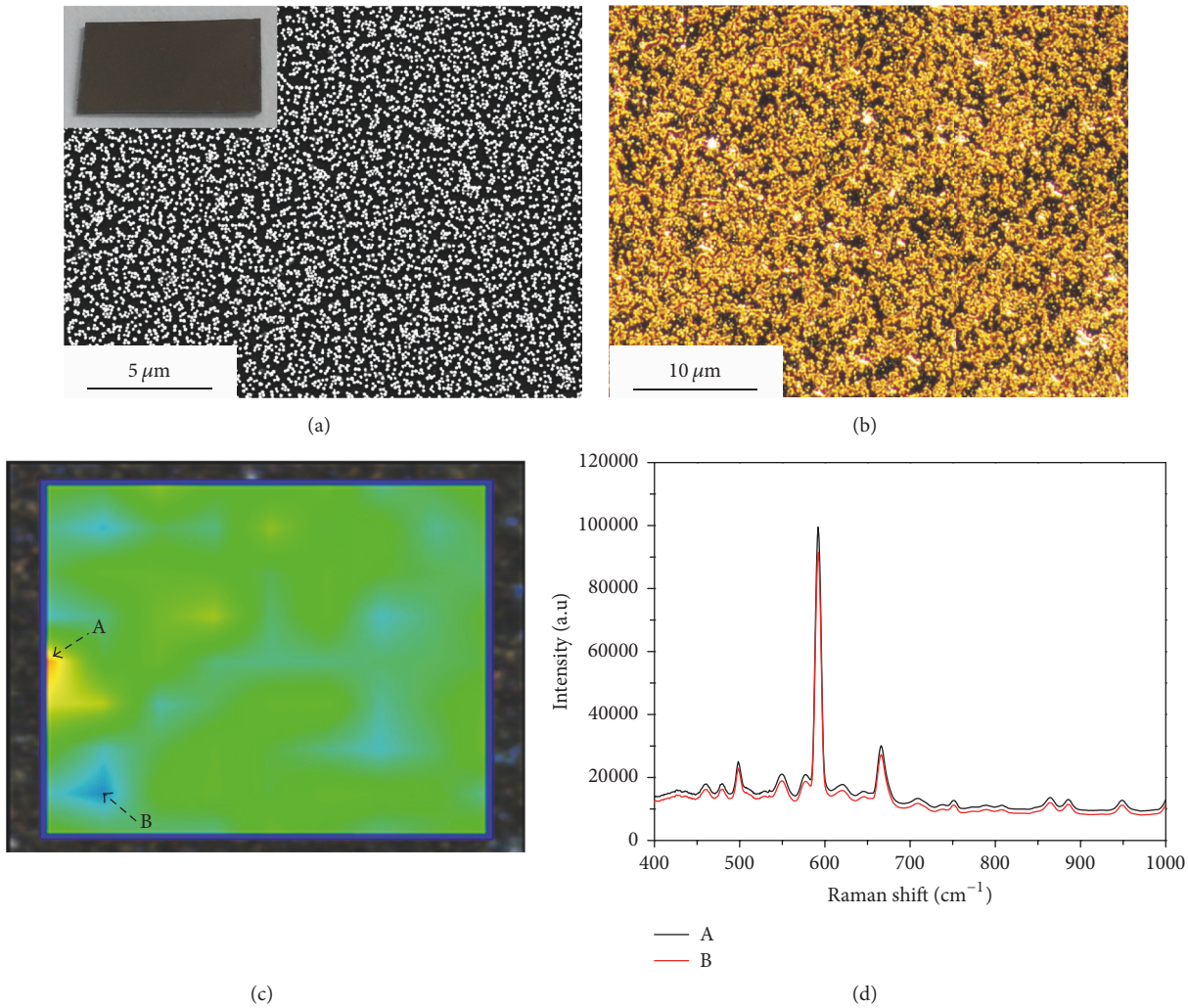

Figure 2: (a) SEM image of the HAuNFs substrates, the inset is digital photograph of substrates. (b) Dark-field image of the HAuNFs substrates. (c) SERS mapping of NBA-labeled HAuNFs substrates at 592 cm^{-1} of the band. (d) SERS spectra at point A and point B in (c).

performed (Figure 4(b)). The Raman shifts at 733 cm^{-1} are attributed to ring breathing mode of adenine [34]. We can see that the detection limit of miR-125a-5p solution is down to 10^{-9} M. Under the concentration of 10^{-9} M, the valid Raman band to identify miR-125a-5p is at 733 cm^{-1}. Thus, the HAuNFs substrates can be employed as a perfect SERS substrate for label-free miRNAs detection at lower concentrations.

SERS spectra were collected for all the miRNAs in the range between 600 and 1700 cm^{-1}. The spectrum of each miRNA was obtained by averaging 10 different points. Figure 5(a) showed a stacked view of normalized mean data for miR-10a-5p, miR-125a-5p, and miR-196a-5p. The intensity of SERS spectrum of miRNA was normalized to get the relative intensity from 0 to 1. There are many characteristic vibrational bands which may be attributed to four RNA bases, such as the peaks at 733 cm^{-1}, 782 cm^{-1} (C (ring breathing modes in the RNA bases)) [34], 1179 cm^{-1} (G, C8-H bending) [35], 1285 cm^{-1} (phosphodiester groups in nucleic acids) [36], and 1575 cm^{-1} (A, G (ring breathing modes of the RNA bases)) [37]. SERS spectra of the three kinds of miRNAs were extremely similar, but they still had differences in the intensities of some characteristic bands. Then, to better compare the SERS spectra differences, the difference spectra among the three kinds of miRNAs were computed, and the results were as follows.

The difference spectra were computed by subtracting the spectrum of miR-125a-5p from the spectrum of miR-196a-5p (miR-125a-5p - miR-196a-5p), the spectrum of miR-10a-5p from the spectrum of miR-196a-5p (miR-10a-5p - miR-196a-5p), and the spectrum of miR-10a-5p from the spectrum of miR-125a-5p (miR-10a-5p - miR-125a-5p). With reference to the Raman band assignments in Table 2, we could assign the characteristic bands in three difference spectra. As shown in Figure 5(b) (miR-125a-5p - miR-196a-5p), we could learn that the positive bands at 733 cm^{-1}, 828 cm^{-1} (O-P-O stretching RNA) [34], 930 cm^{-1}(Ribose vibration, one of the distinct RNA modes) [37], 1071 cm^{-1} (PO^{2-}, symm, stretching) [34], 1223 cm^{-1} (A concerted ring mode (RNA)) [34], 1507 cm^{-1},

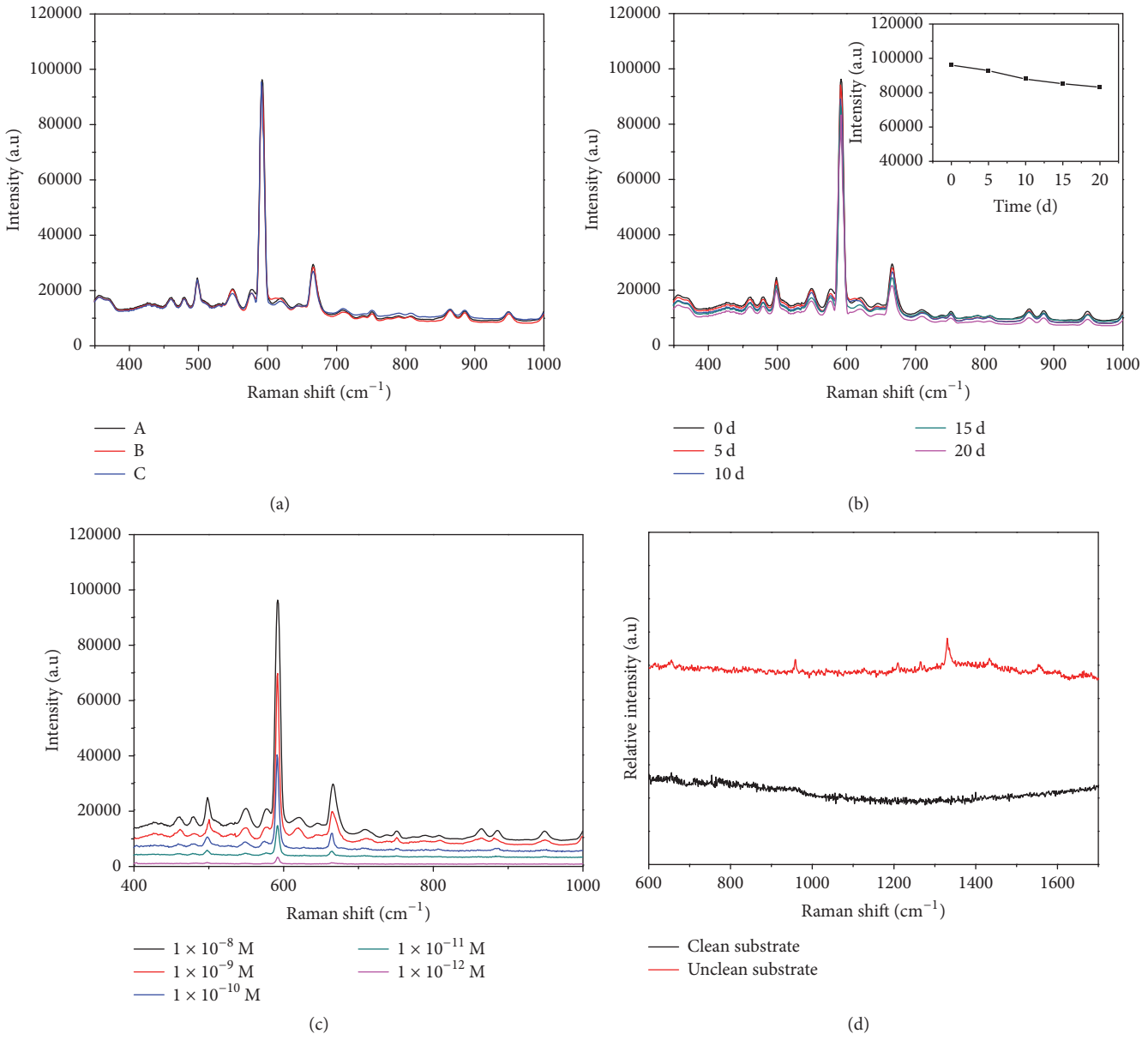

Figure 3: (a) The reproducibility of HAuNFs substrates measured with NBA (1×10^{-8} M). (b) SERS stability of NBA-labeled HAuNFs substrates measured with NBA (1×10^{-8} M). HAuNFs substrates were stored for several days at room temperature. Inset image was SERS intensities of the bands at 592 cm^{-1} corresponding to the SERS spectra (b). (c) SERS spectra of HAuNFs substrates measured with NBA from 1×10^{-8} M to 1×10^{-12} M. (d) SERS spectra of (black curve) HAuNFs substrates treated with 0.1 M KI and (red curve) HAuNFs substrates without being treated with 0.1 M KI.

and 1575 cm^{-1} were from the spectrum of miR-125a-5p, indicating that the relative intensity of these bands which were mainly the vibration bands of adenine and cytosine was higher in the spectrum of miR-125a-5p when compared with that of miR-196a-5p, whereas the negative bands for Figure 5(b) at 1320 cm^{-1} (G (RNA)) [34], 1443 cm^{-1} (nucleic acid modes) [38], and 1655 cm^{-1} (U (C=O symmetric stretch modes of the RNA bases)) [37] were from the spectrum of miR-196a-5p. These peaks were mainly generated by the vibration peaks of guanine and uracil. In Figure 5(c), the difference spectra between miR-10a-5p and miR-196a-5p that yielded the positive bands at 930 cm^{-1}, 1071 cm^{-1}, 1179 cm^{-1}, 1263 cm^{-1}, 1342 cm^{-1}, 1507 cm^{-1}, and 1546 cm^{-1} (ring breathing modes in the RNA bases) [39] were from the spectrum of miR-10a-5p. The majority of these peaks could be assigned as adenine. The negative bands at 782 cm^{-1}, 1120 cm^{-1}, 1320 cm^{-1}, and 1655 cm^{-1} were from the spectrum of miR-196a-5p, which could be similarly assigned as guanine and uracil. Furthermore, Figure 5(d) (miR-10a-5p - miR-125a-5p) showed that positive bands at 828 cm^{-1}, 1179 cm^{-1},

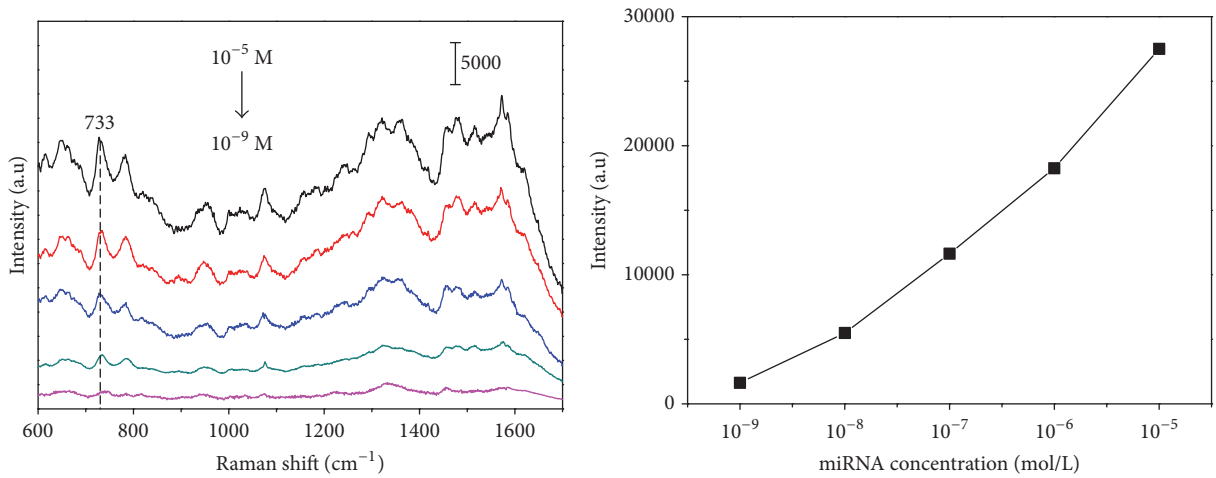

Figure 4: (a) SERS spectra of miR-125a-5p with different concentrations (10^{-5}, 10^{-6}, 10^{-7}, 10^{-8}, and 10^{-9} M) on the HAuNFs substrates. (b) SERS intensity at 733 cm^{-1} for miR-125a-5p with different concentrations shown in Figure 4(a).

Table 2: Assignment of corresponding SERS bands.

Raman band (cm^{-1})	Assignment
733	A (ring breathing mode of RNA bases)
782	C (ring breathing modes in the RNA bases)
828	O-P-O stretching RNA
930/974	Ribose vibration, one of the distinct RNA modes
1060–1095	PO^{2-}, symm, stretching
1120	The strong C-O band of ribose (RNA)
1179	G, C8-H bending
1223	A concerted ring mode (RNA)
1263	A (ring breathing modes of the RNA bases)
1285	Phosphodiester groups in nucleic acids
1320/1342	G (RNA)
1443	Nucleic acid modes
1507	A (ring breathing modes in the RNA bases)
1546	Ring breathing modes in the RNA bases
1575	G (ring breathing modes of the RNA bases)
1655–1680	U, C (C=O symmetric stretch modes of the RNA bases)

1285 cm^{-1}, and 1546 cm^{-1} were from the spectrum of miR-10a-5p, and negative bands at 782 cm^{-1}, 974 cm^{-1}, 1060 cm^{-1}, 1263 cm^{-1}, and 1575 cm^{-1} were from the spectrum of miR-125a-5p.

To further compare and quantize the differences of miR-10a-5p, miR-125a-5p, and miR-196a-5p, based on the normalized mean SERS spectra of each miRNA, we compared the mean relative intensity at four different Raman bands, including 733 cm^{-1}, 1085 cm^{-1}, 1575 cm^{-1}, and 1655 cm^{-1}. As shown in Figure 6, miR-125a-5p showed the higher relative intensity at 733 cm^{-1} and 1575 cm^{-1} than miR-10a-5p and miR-196a-5p. However, the relative intensity of Raman bands at 1085 cm^{-1} and 1655 cm^{-1} for miR-125a-5p is lower than that of miR-10a-5p and miR-196a-5p. Furthermore, there are also some differences between miR-10a-5p and miR-196a-5p. The relative intensity of Raman bands at 733 cm^{-1}, 1085 cm^{-1}, and 1655 cm^{-1} was significantly higher and there was no significance at 1575 cm^{-1} for miR-196a-5p as compared to miR-10a-5p. Based on the above analysis, we could learn that the result is consistent with these miRNAs sequences in Table 1.

3.4. PCA Analysis. In order to determine if SERS spectra could be used to distinguish among these miRNAs, we employed PCA for fine analysis of the spectral data. PCA is a multivariate statistical analysis method, by which large spectral data are reduced into small number of independent variables such as principal components (PCs) and contributions of these factors in a given spectra are known as scores. Scores of PCs are one of the parameters widely used

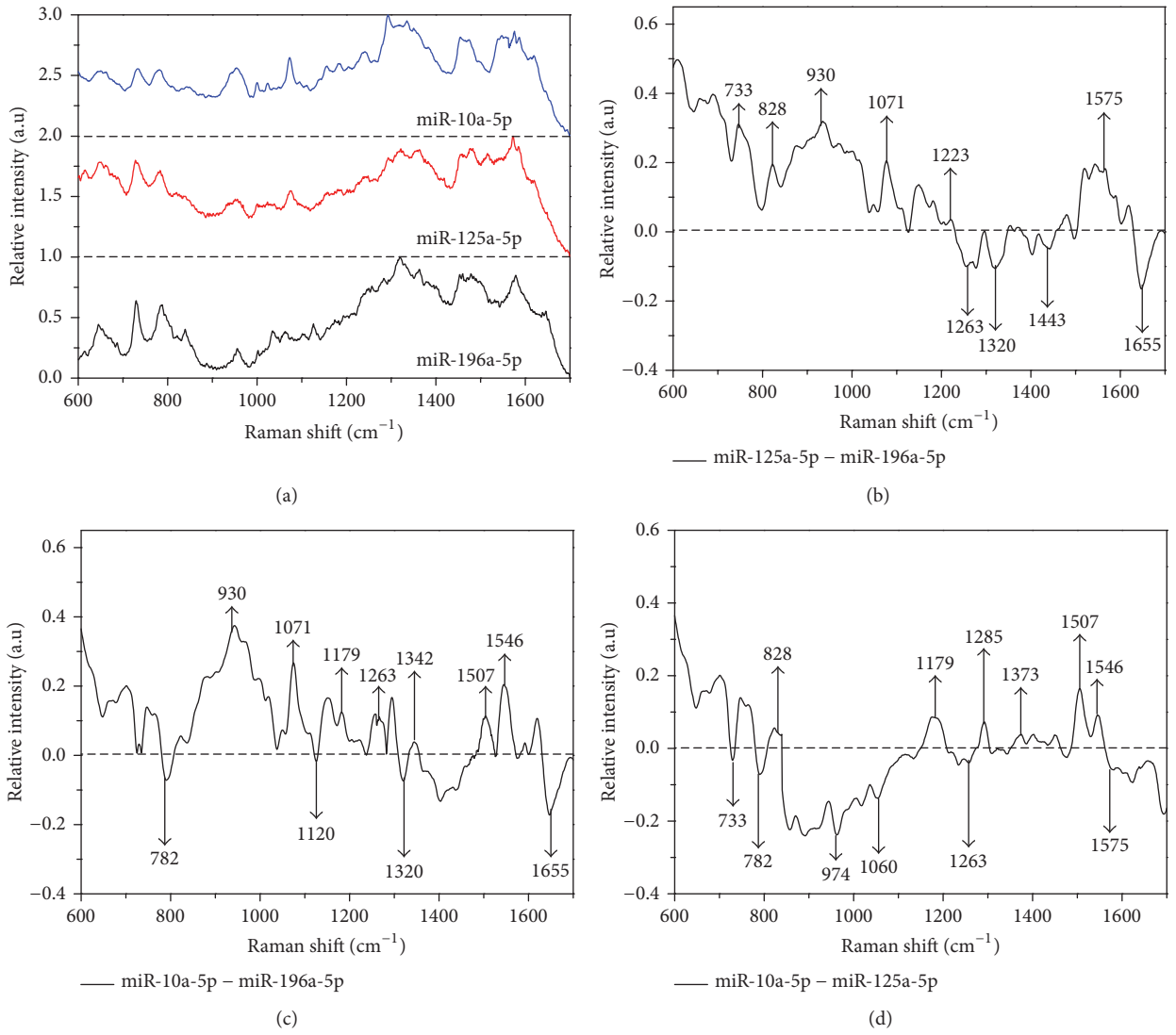

FIGURE 5: (a) The normalized mean SERS spectra of miR-10a-5p, miR-125a-5p, and miR-196a-5p. Difference spectra among three kinds of miRNAs were computed: (b) miR-125a-5p − miR-196a-5p, (c) miR-10a-5p − miR-196a-5p, and (d) miR-10a-5p − miR-125a-5p.

for classification [40, 41]. Figure 7 showed the scatter plots of the SERS spectra for three kinds of miRNAs projected into a two-dimensional subspace using principal component scores PC1 and PC2. It is seen that the PC1 possesses 64.5% variation, PC2 16.7% variation. In Figure 7, each spot represents the average SERS spectrum of miRNA tested once. PCA plots indicated that these miRNAs are well divided into three distinct groups. The intrinsic difference in composition and concentration of four bases for different miRNAs will cause the groups to be separated from each other. PCA gives more intuitive results than direct analysis spectral difference among these miRNAs. The results suggested that PCA can easily classify the miRNAs based on their specific spectral features. Although the traditional miRNA detection technologies are valuable for the treatment and diagnosis in cancer and disease, they have limited sensitivity and are time-consuming. The SERS method described in this study overcomes these limitations because it enables rapid and specific miRNA detection, provides a molecular fingerprint of individual miRNA analytes, and offers a better understanding of specific miRNA spectral characteristics to facilitate data interpretation.

4. Conclusions

In conclusion, we developed an simple, sensitive, and label-free method for detection and identification of miRNAs based on HAuNFs substrates. These substrates with good reproducible, uniform, and high SERS effect were prepared by the electrostatically assisted APTES-functionalized surface-sedimentary self-assembly method. Using HAuNFs substrate as a high-performance sensing platform, SERS spectra of miRNAs represented much significant peaks and strong signals. The differences in SERS spectral among three kinds of miRNAs revealed their intrinsic difference in composition

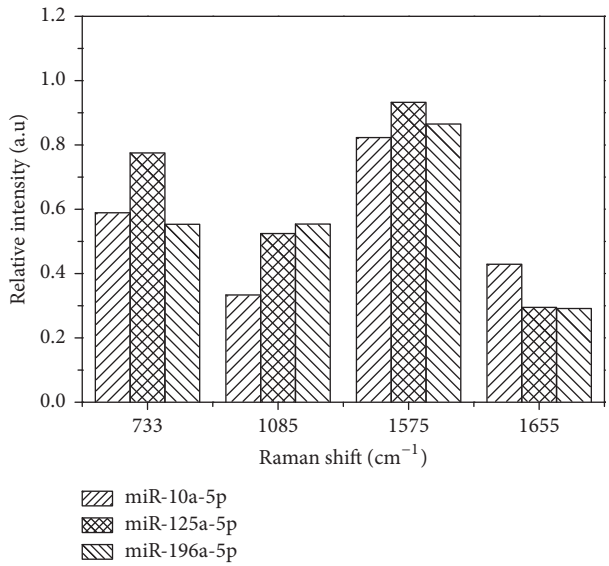

Figure 6: The comparison of mean relative intensity at four different Raman bands among miR-10a-5p, miR-125a-5p, and miR-196a-5p.

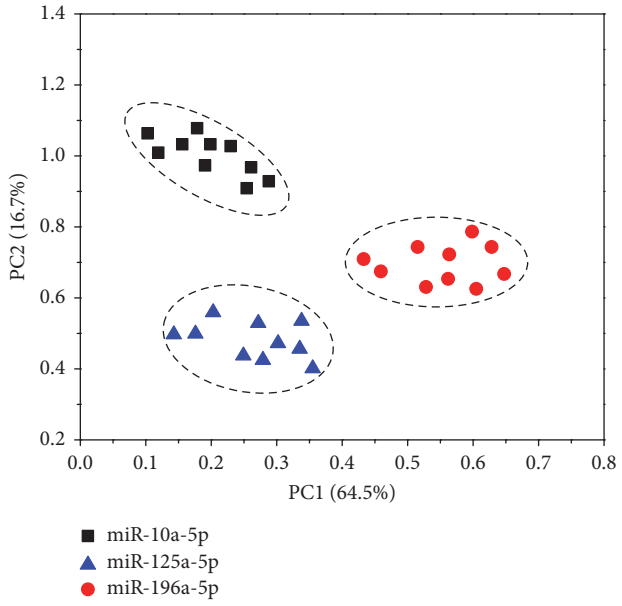

Figure 7: PCA scores plot of SERS spectra for three kinds of miRNAs. Each miRNA was coded by different color.

and concentration of four RNA bases. PCA achieved a successful segregation of miRNAs based on their SERS spectra. This novel application for SERS provides an important advancement in miRNA detection and has the capacity to dramatically advance our understanding of the role for miRNAs in disease pathogenesis.

Conflicts of Interest

The authors declare that they have no conflicts of interest.

Authors' Contributions

Xiaowei Cao and Min Bao contributed equally to this work.

Acknowledgments

The authors gratefully acknowledge support from the National Natural Science Foundation of China (Grant 81370118), the China Postdoctoral Science Foundation (Grant 2017M611927), Natural Science Fund for Colleges and Universities in Jiangsu Province (Grant 17KJB416012), Clinical Medicine Science and Technology Projects of Jiangsu Province (Grant 2013023), and Jiangsu Province Graduate Education Innovation Project (Grant KYLX16-1410).

References

[1] D. P. Bartel, "MicroRNAs: genomics, biogenesis, mechanism, and function," *Cell*, vol. 116, no. 2, pp. 281–297, 2004.

[2] B. P. Lewis, C. B. Burge, and D. P. Bartel, "Conserved seed pairing, often flanked by adenosines, indicates that thousands of human genes are microRNA targets," *Cell*, vol. 120, no. 1, pp. 15–20, 2005.

[3] E. Berezikov, G. Van Tetering, M. Verheul et al., "Many novel mammalian microRNA candidates identified by extensive cloning and RAKE analysis," *Genome Research*, vol. 16, no. 10, pp. 1289–1298, 2006.

[4] S. Gilad, E. Meiri, Y. Yogev et al., "Serum microRNAs are promising novel biomarkers," *PLoS ONE*, vol. 3, no. 9, Article ID e3148, 2008.

[5] A. L. Kasinski and F. J. Slack, "MicroRNAs en route to the clinic: Progress in validating and targeting microRNAs for cancer therapy," *Nature Reviews Cancer*, vol. 11, no. 12, pp. 849–864, 2011.

[6] C. M. Croce, "Causes and consequences of microRNA dysregulation in cancer," *Nature Reviews Genetics*, vol. 10, no. 10, pp. 704–714, 2009.

[7] R. Huo, M. Dai, Y. Fan, L. Li, and J. Zu, "Predictive value of miRNA-29a and miRNA-10a-5p for 28-day mortality in patients with sepsis-induced acute kidney injury," *Nan Fang Yi Ke Da Xue Xue Bao*, vol. 37, no. 5, pp. 646–651, 2017.

[8] Y. Zhi, X. Xie, R. Wang et al., "Serum level of miR-10-5p as a prognostic biomarker for acute myeloid leukemia," *International Journal of Hematology*, vol. 102, no. 3, pp. 296–303, 2015.

[9] A. Safari, M. Seifoleslami, E. Yahaghi, F. Sedaghati, and M. K. Khameneie, "Upregulation of miR-20a and miR-10a expression levels act as potential biomarkers of aggressive progression and poor prognosis in cervical cancer," *Tumor Biology*, pp. 1–5, 2015.

[10] M.-J. Long, F.-X. Wu, P. Li, M. Liu, X. Li, and H. Tang, "MicroRNA-10a targets CHL1 and promotes cell growth, migration and invasion in human cervical cancer cells," *Cancer Letters*, vol. 324, no. 2, pp. 186–196, 2012.

[11] L. Zhong, S. Sun, J. Shi et al., "MicroRNA-125a-5p plays a role as a tumor suppressor in lung carcinoma cells by directly targeting STAT3," *Tumour Biology the Journal of the International Society for Oncodevelopmental Biology & Medicine*, vol. 39, no. 6, pp. 1–11, 2017.

[12] H. He, F. Xu, W. Huang et al., "miR-125a-5p expression is associated with the age of breast cancer patients," *Genetics & Molecular Research Gmr*, vol. 14, no. 4, pp. 17927–17933, 2015.

[13] H.-L. Li, S.-P. Xie, Y.-L. Yang et al., "Clinical significance of upregulation of mir-196a-5p in gastric cancer and enriched KEGG pathway analysis of target genes," *Asian Pacific Journal of Cancer Prevention*, vol. 16, no. 5, pp. 1781–1787, 2015.

[14] J. D. Driskell, A. G. Seto, L. P. Jones et al., "Rapid microRNA (miRNA) detection and classification via surface-enhanced Raman spectroscopy (SERS)," *Biosensors and Bioelectronics*, vol. 24, no. 4, pp. 917–922, 2008.

[15] K. A. Willets, "Surface-enhanced Raman scattering (SERS) for probing internal cellular structure and dynamics," *Analytical and Bioanalytical Chemistry*, vol. 394, no. 1, pp. 85–94, 2009.

[16] J.-Y. Huang, C. Zong, L.-J. Xu, Y. Cui, and B. Ren, "Clean and modified substrates for direct detection of living cells by surface-enhanced Raman spectroscopy," *Chemical Communications*, vol. 47, no. 20, pp. 5738–5740, 2011.

[17] H. Zhou, D. Yang, N. P. Ivleva, N. E. Mircescu, R. Niessner, and C. Haisch, "SERS detection of bacteria in water by in situ coating with Ag nanoparticles," *Analytical Chemistry*, vol. 86, no. 3, pp. 1525–1533, 2014.

[18] A. M. Gabudean, M. Focsan, and S. Astilean, "Gold nanorods performing as dual-modal nanoprobes via metal-enhanced fluorescence (MEF) and surface-enhanced Raman scattering (SERS)," *The Journal of Physical Chemistry C*, vol. 116, no. 22, pp. 12240–12249, 2012.

[19] T. A. Nguyen and S. W. Lee, "Effect of electrodeposition cycles on the performance of gold nanostructures as SERS-active substrates," *Industrial & Engineering Chemistry Research*, vol. 48, no. 25, pp. 230–234, 2017.

[20] Y. Fu, J. Zhang, and J. R. Lakowicz, "Rational design of Raman-labeled nanoparticles for a dual-modality, light scattering immunoassay on a polystyrene substrate," *Chemical Communications*, vol. 48, no. 78, pp. 9726–9728, 2012.

[21] E. Hao, S. Li, R. C. Bailey, S. Zou, G. C. Schatz, and J. T. Hupp, "Optical properties of metal nanoshells," *The Journal of Physical Chemistry B*, vol. 108, no. 4, pp. 1224–1229, 2004.

[22] C. Y. Song, N. Zhou, B. Y. Yang, Y. J. Yang, and L. H. Wang, "Facile synthesis of hydrangea flower-like hierarchical gold nanostructures with tunable surface topographies for single-particle surface-enhanced Raman scattering," *Nanoscale*, vol. 7, no. 40, pp. 17004–17011, 2015.

[23] L.-J. Xu, Z.-C. Lei, J. Li, C. Zong, C. J. Yang, and B. Ren, "Label-free surface-enhanced Raman spectroscopy detection of DNA with single-base sensitivity," *Journal of the American Chemical Society*, vol. 137, no. 15, pp. 5149–5154, 2015.

[24] I. R. Nabiev, H. Morjani, and M. Manfait, "Selective analysis of antitumor drug interaction with living cancer cells as probed by surface-enhanced Raman spectroscopy," *European Biophysics Journal*, vol. 19, no. 6, pp. 311–316, 1991.

[25] B. N. Khlebtsov, V. A. Khanadeev, E. V. Panfilova, D. N. Bratashov, and N. G. Khlebtsov, "Gold nanoisland films as reproducible SERS substrates for highly sensitive detection of fungicides," *ACS Applied Materials & Interfaces*, vol. 7, no. 12, pp. 6518–6529, 2015.

[26] Y. Sun, L. Xu, F. Zhang et al., "A promising magnetic SERS immunosensor for sensitive detection of avian influenza virus," *Biosensors and Bioelectronics*, vol. 89, pp. 906–912, 2017.

[27] L. Ouyang, Y. Hu, L. Zhu, G. J. Cheng, and J. Irudayaraj, "A reusable laser wrapped graphene-Ag array based SERS sensor for trace detection of genomic DNA methylation," *Biosensors and Bioelectronics*, vol. 92, pp. 755–762, 2017.

[28] E. Le Ru, E. Blackie, M. Meyer, and P. G. Etchegoint, "Surface enhanced raman scattering enhancement factors: a comprehensive study," *The Journal of Physical Chemistry C*, vol. 111, no. 37, pp. 13794–13803, 2007.

[29] M. Fan, F. J. Lai, H. L. Chou, W. Lu, B. J. Hwang, and A. G. Brolo, "Surface-enhanced Raman scattering (SERS) from Au: Ag bimetallic nanoparticles: the effect of the molecular probe," *Chemical Science*, vol. 4, no. 1, pp. 509–515, 2013.

[30] E. Nalbant Esenturk and A. R. Hight Walker, "Surface-enhanced Raman scattering spectroscopy via gold nanostars," *Journal of Raman Spectroscopy*, vol. 40, no. 1, pp. 86–91, 2009.

[31] Q. Q. Su, X. Y. Ma, J. Dong, C. Y. Jiang, and W. P. Qian, "A reproducible SERS substrate based on electrostatically assisted aptes-functionalized surface-assembly of gold nanostars," *Applied Materials & Interfaces*, vol. 3, no. 6, pp. 1873–1879, 2011.

[32] K. C. Grabar, P. C. Smith, M. D. Musick et al., "Kinetic control of interparticle spacing in Au colloid-based surface: Rational nanometer-scale architecture," *Journal of the American Chemical Society*, vol. 118, no. 5, pp. 1148–1153, 1996.

[33] F. Wei, D. Zhang, N. J. Halas, and J. D. Hartgerink, "Aromatic amino acids providing characteristic motifs in the raman and SERS spectroscopy of peptides," *The Journal of Physical Chemistry B*, vol. 112, no. 30, pp. 9158–9164, 2008.

[34] I. Notingher, C. Green, C. Dyer et al., "Discrimination between ricin and sulphur mustard toxicity in vitro using Raman spectroscopy," *Journal of the Royal Society Interface*, vol. 1, no. 1, pp. 79–90, 2004.

[35] N. Fujimoto, A. Toyama, and H. Takeuchi, "Effects of hydrogen bonding on the UV resonance Raman bands of the adenine ring and its C8-deuterated analog," *Journal of Molecular Structure*, vol. 447, no. 1-2, pp. 61–69, 1998.

[36] R. K. Dukor, "Vibrational spectroscopy in the detection of cancer," *Biomedical Applications*, vol. 5, pp. 3335–3359, 2002.

[37] J. W. Chan, D. S. Taylor, T. Zwerdling, S. M. Lane, K. Ihara, and T. Huser, "Micro-raman spectroscopy detects individual neoplastic and normal hematopoietic cells," *Biophysical Journal*, vol. 90, no. 2, pp. 648–656, 2006.

[38] N. Stone, C. Kendall, J. Smith, P. Crow, and H. Barr, "Raman spectroscopy for identification of epithelial cancers," *Faraday Discussions*, vol. 126, pp. 141–157, 2004.

[39] R. Malini, K. Venkatakrishna, J. Kurien et al., "Discrimination of normal, inflammatory, premalignant, and malignant oral tissue: A Raman spectroscopy study," *Biopolymers*, vol. 81, no. 3, pp. 179–193, 2006.

[40] H. Yao, Z. Tao, M. Ai et al., "Raman spectroscopic analysis of apoptosis of single human gastric cancer cells," *Vibrational Spectroscopy*, vol. 50, no. 2, pp. 193–197, 2009.

[41] G. D. McEwen, Y. Z. Wu, M. J. Tang et al., "Subcellular spectroscopic markers, topography and nanomechanics of human lung cancer and breast cancer cells examined by combined confocal Raman microspectroscopy and atomic force microscopy," *Analyst*, vol. 138, no. 3, pp. 787–797, 2013.